5.0 Principle of Muon Spin Rotation/Relaxation/Resonance

The expression μSR is the acronym for Muon Spin Rotation/Relaxation/Resonance and underlines the analogy with NMR (Nuclear Magnetic Resonance). There are, however, important differences (see key features of μSR, next page). For instance with μSR it is possible to perform measurements without applying a magnetic field (so called zero field μSR, ZF) a big advantage with respect to NMR because this allows to investigate magnetic systems without perturbation. NQR (Nuclear Quadrupole Resonance) is also a zero field technique, but for magnetic investigations less direct than zero field μSR.

The method is based on the observation of the time evolution of the polarization P(t) of an ensemble of muons implanted in a sample. This quantity contains the physical information about the interaction of the muon magnetic moment with its local environment. P(t) is obtained from the intensity of decay positrons as a function of time after implantation.

The muon acts as a local very sensitive magnetic probe. Value ($\omega_L = \gamma_\mu B_{loc}$), direction, distribution and dynamics of internal (microscopic) magnetic fields can be measured. Such fields may be produced by electronic moments, nuclear moments or local currents as those in superconductors). With μSR it is also possible to determine magnetic, non magnetic, and superconducting fractions. Muonium acts as a Hydrogen isotope, e.g., in chemical reactions or as impurity in semiconductors and insulators and gives information about its electronic environment.

In a μSR experiment one measures the positron rate with scintillators, which are placed around the sample.

The positron is emitted preferentially in the spin direction of the muon at the moment of the decay.

$$\frac{dN_{e^+}}{d\Omega} \propto (1 + AP\cos\theta) = (1 + A\vec{P}(t)\cdot\vec{n}) \qquad [5\text{-}1]$$

A: Asymmetry parameter (the theoretical decay asymmetry averaged over the positron energy is 1/3).

After detecting the positrons from several 10^6 stopped muons, one obtains histograms as in Fig. 5-1, which in the ideal case have following dependence (t=0 is the implantation time, N_{bg} is a time independent background):

$$N_{e^+}(t) = N_0 e^{-\frac{t}{\tau_\mu}}(1 + A_0\vec{P}(t)\hat{n}) + N_{bg} \qquad [5\text{-}2]$$

The recorded events in the positron histograms reflect the time evolution of the polarization of the muon ensemble.

Key features of μSR

Muons are **purely magnetic** probes (I = ½, no quadrupolar effects[1])

Local information, mainly **interstitial** probe → complementary to NMR

Large magnetic moment: $\mu_\mu = 3.18\ \mu_p = 8.89\ \mu_n$ → **sensitive** probe

Particularly suitable for:
Very weak effects, small moment magnetism ~ $10^{-3}\ \mu_B$ /Atom
Random magnetism (e.g. spin glasses)
Short range order (where neutron scattering is not sensitive)

Independent determination of **magnetic moment** and of **magnetic volume fraction**

Determination of magnetic/non-magnetic/superconducting fractions

Full polarization in zero field, independent of temperature → unique measurements without disturbance of the system (typical polarization in NMR $< I_z >= \frac{\gamma\hbar I(I+1)}{3k_B T} B$ is very small.

Needs high magnetic fields and low temperatures)

Single particle detection → extremely high sensitivity

No restrictions in choice of materials to be studied

Fluctuation time window: $10^{-5} < t < 10^{-11}$ s

Bound state: μ^+e^- Muonium, used as H-Isotope for spectroscopy, impurity studies, radical chemistry, reaction kinetics

Other features:

Number of implanted muons << number of atoms → negligible sample damage
No perturbation of the system (unlike spin probes in EPR)
No special isotope is needed (as in NMR, Mössbauer)

[1] $Q =< I, M_I = I \left| 3z^2 - r^2 \right| I, M_I = I >$ since $3z^2 - r^2 \propto Y_{2,0}$ (irreducible tensor operator), by Wigner-Eckart theorem: $Q =< I, I \left| 3z^2 - r^2 \right| I, I >= C < I, I \left| 3I_z^2 - I^2 \right| I, I >= C \cdot I(2I-1)$, i.e. Q=0 for I=0 or I=1/2 (see C. Slichter, Principles of Magnetic Resonance, Chapter 9).

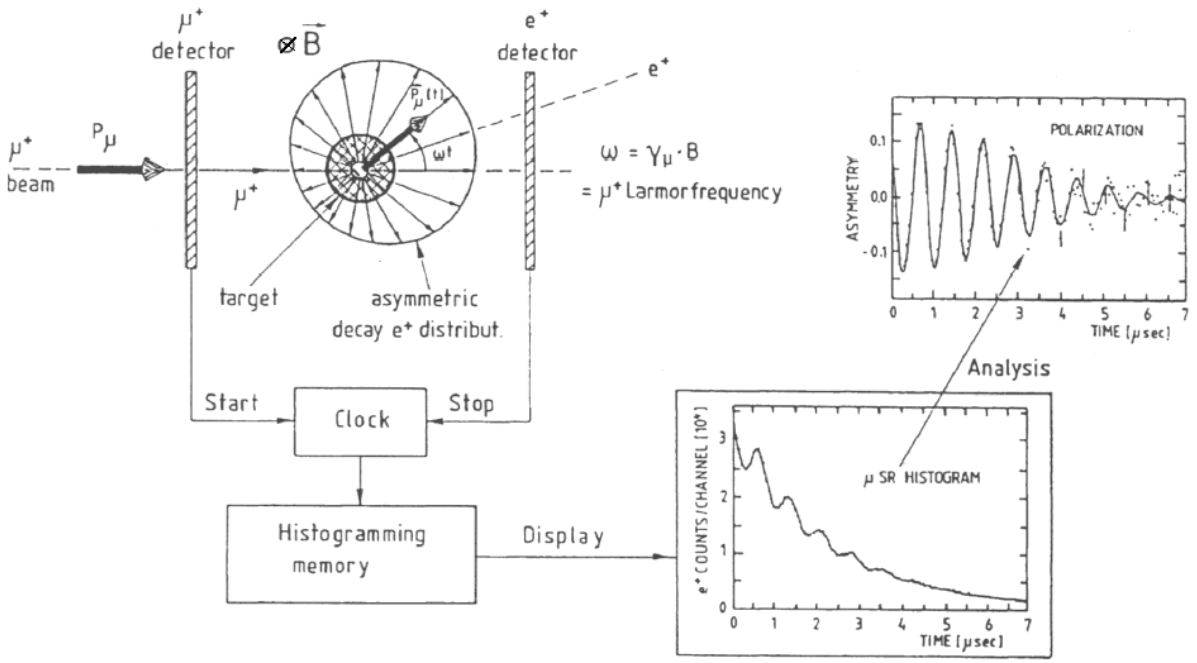

Fig 5-1: Principle of a μSR-measurement in transverse field (TF) (Time differential μSR).

a)

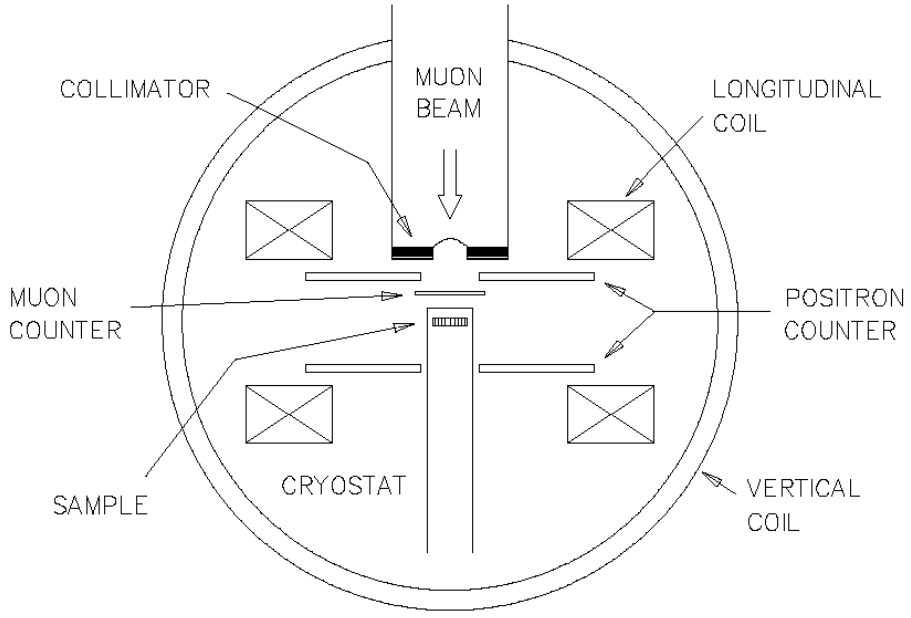

b)

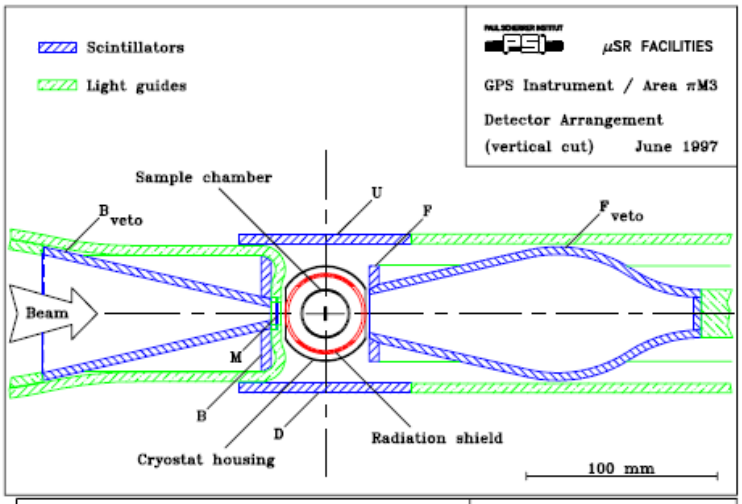
Scintillators
Light guides
μSR FACILITIES
GPS Instrument / Area πM3
Detector Arrangement
(vertical cut) June 1997
Sample chamber
U
B veto
F
F veto
Beam
M
B
D
Cryostat housing
Radiation shield
100 mm

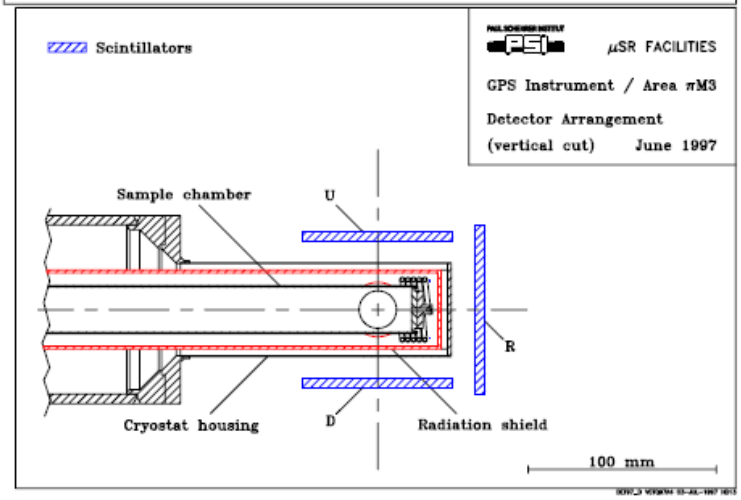
Scintillators
μSR FACILITIES
GPS Instrument / Area πM3
Detector Arrangement
(vertical cut) June 1997
Sample chamber
U
R
Cryostat housing
D
Radiation shield
100 mm

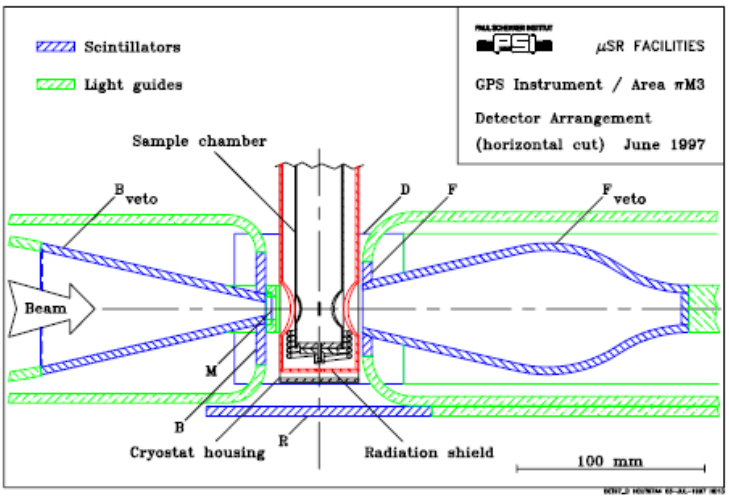
Scintillators
Light guides
μSR FACILITIES
GPS Instrument / Area πM3
Detector Arrangement
(horizontal cut) June 1997
Sample chamber
B veto
D
F
F veto
Beam
M
B
R
Cryostat housing
Radiation shield
100 mm

c)

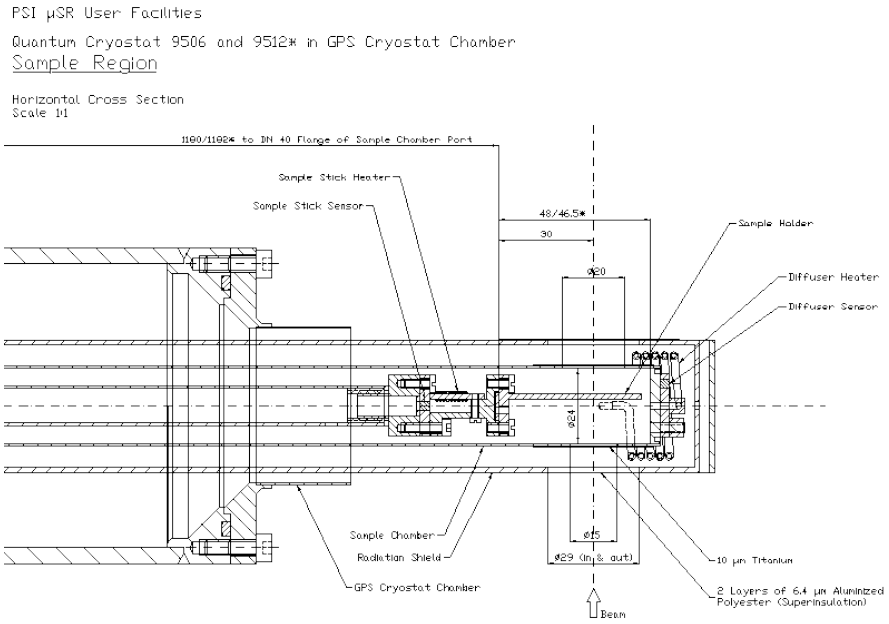

Fig 5-2: a) Schematic of a µSR apparatus, top view. b) Detailed view of detectors and c) sample region of the General Purpose Spectrometer (GPS) at PSI.

One distinguishes between continuous muon beams (PSI and TRIUMF, Canada) and pulsed beams (ISIS/RAL, UK and J-PARC, Japan).
At PSI the accelerator time structure (50 MHz microstructure) and the pion lifetime (26 ns) leads to a practically continuous surface muon beam:

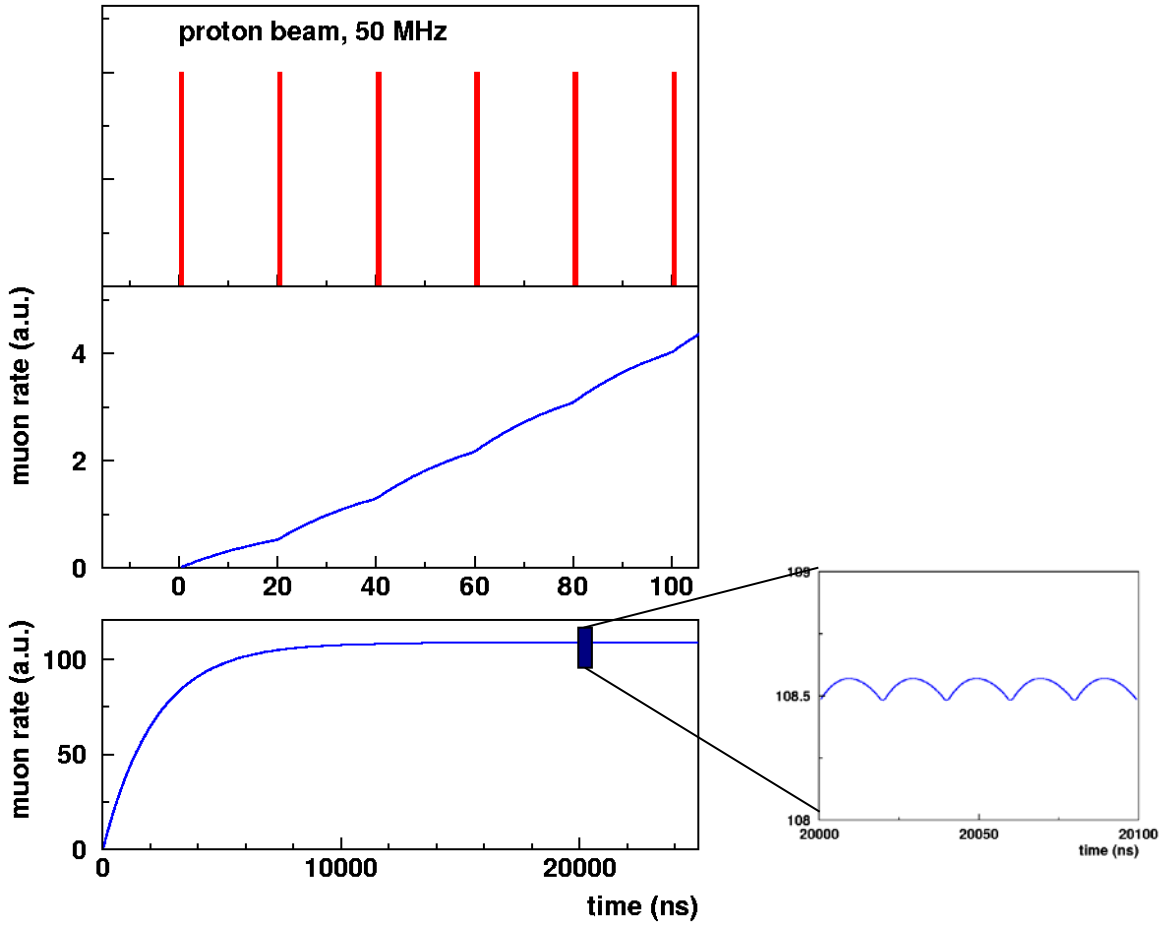

Fig. 5-3: Build-up of the muon rate at PSI.

In a μSR experiment with continuous beam one has to take care that only one muon at a time is present in the sample before decaying, otherwise the time correlation between muon and its decay positron is lost (see Fig. 5-1):

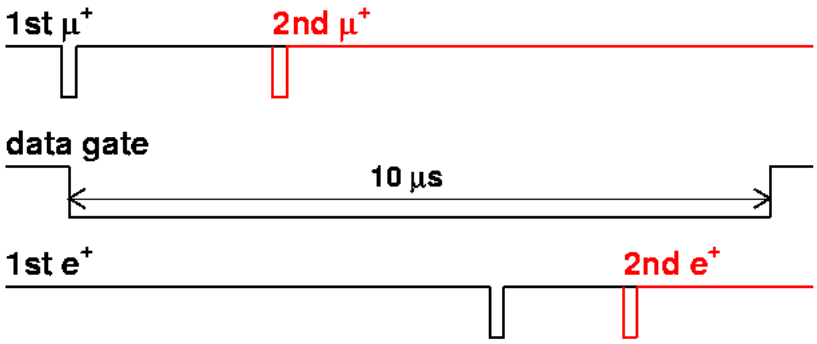

1st μ^+: there was no other μ^+ for at least 10μs in the past

Good Event = (data gate) • (1st e^+) • (no 2nd μ^+) • (no 2nd e^+)

$$R_{acc} = R_\mu \times \exp(-2\Delta t\, R_\mu),\ \Delta t = 10\ \mu s$$

This is done electronically (rejection of second muon event by pileup and busy gate) and by limiting the incoming muon rate.

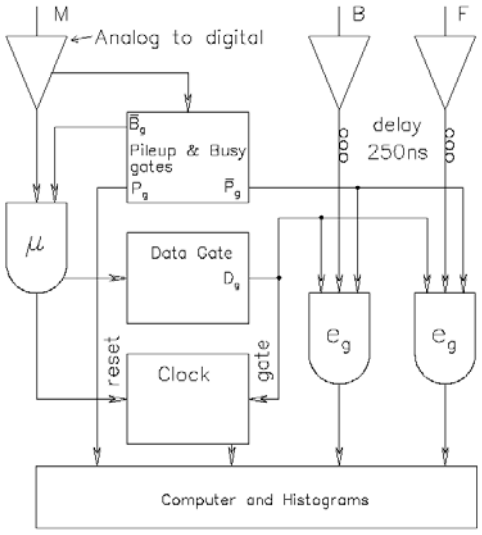

Fig 5-4: Electronic diagram of a μSR experiment at a continuous muon beam facility such as PSI.

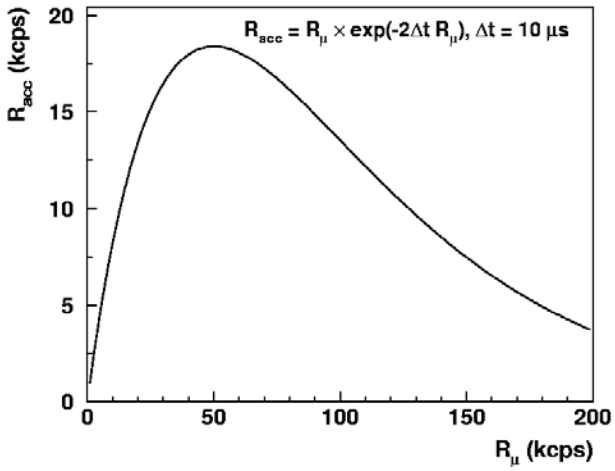

Fig. 5-5: Accepted rate as a function of incoming rate for a time window of 10 µs
($\exp(-2\Delta t R_\mu)$ is the probability that there is no second event in an interval Δt if the rate is R_μ).

At a pulsed machine all the muons are contained in a pulse (50-100 ns wide) with low repetition rate (25-50 Hz). All the decay positrons of a pulse are measured at once. This allows a higher rate. However, one has to take care either to have only one positron in a detector within the observation time, or if there are more than one to get the time stamp for each one. This requires a high segmentation of the positron spectrometer.
A big disadvantage of a pulsed machine is that the time resolution is given by the pulse width (50-100 ns), whereas at a continuous beam line the time resolution is determined by the muon counter which is typically 1 ns or better.
A pulsed beam has in principle a lower background than a continuous beam and allows a better exploitation of a pulsed environment. At PSI, the so-called muon on request electrostatic kicker device (MORE) allows only one muon at the time in the apparatus. This reduces the background, while keeping the excellent time resolution of the continuous beam.

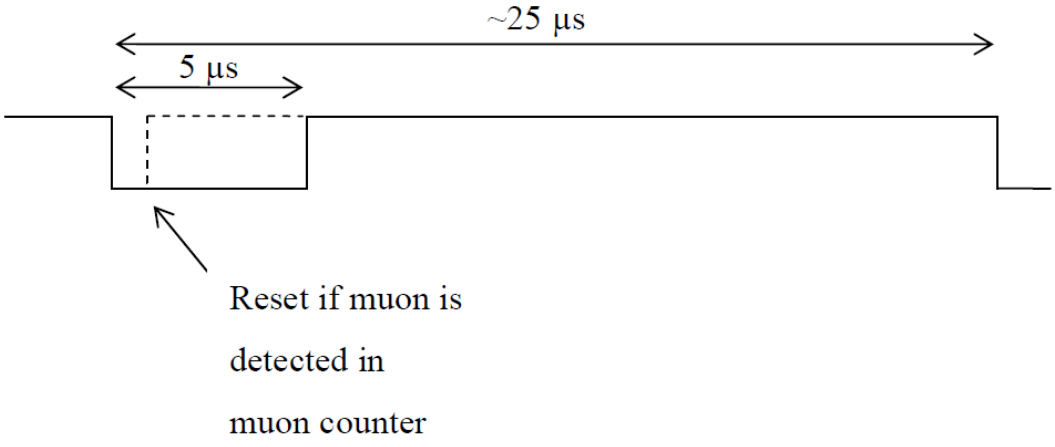

In the MORE mode the muon detector (M-counter) in the spectrometer (GPS or LTF) is used

to trigger the kicker. The kicker is switched to the spectrometer running in "MORE mode" (say, GPS) for a maximum of 5µs at a fixed repetition rate (max. 40 kHz). The signal of the first muon hitting the trigger detector (M-counter) after a minimum delay of 200ns is used to switch the kicker back to the spectrometer running in "parasitic mode" (Low Temperature Facility, LTF in this case). The delay is necessary to avoid damage to the power switches.

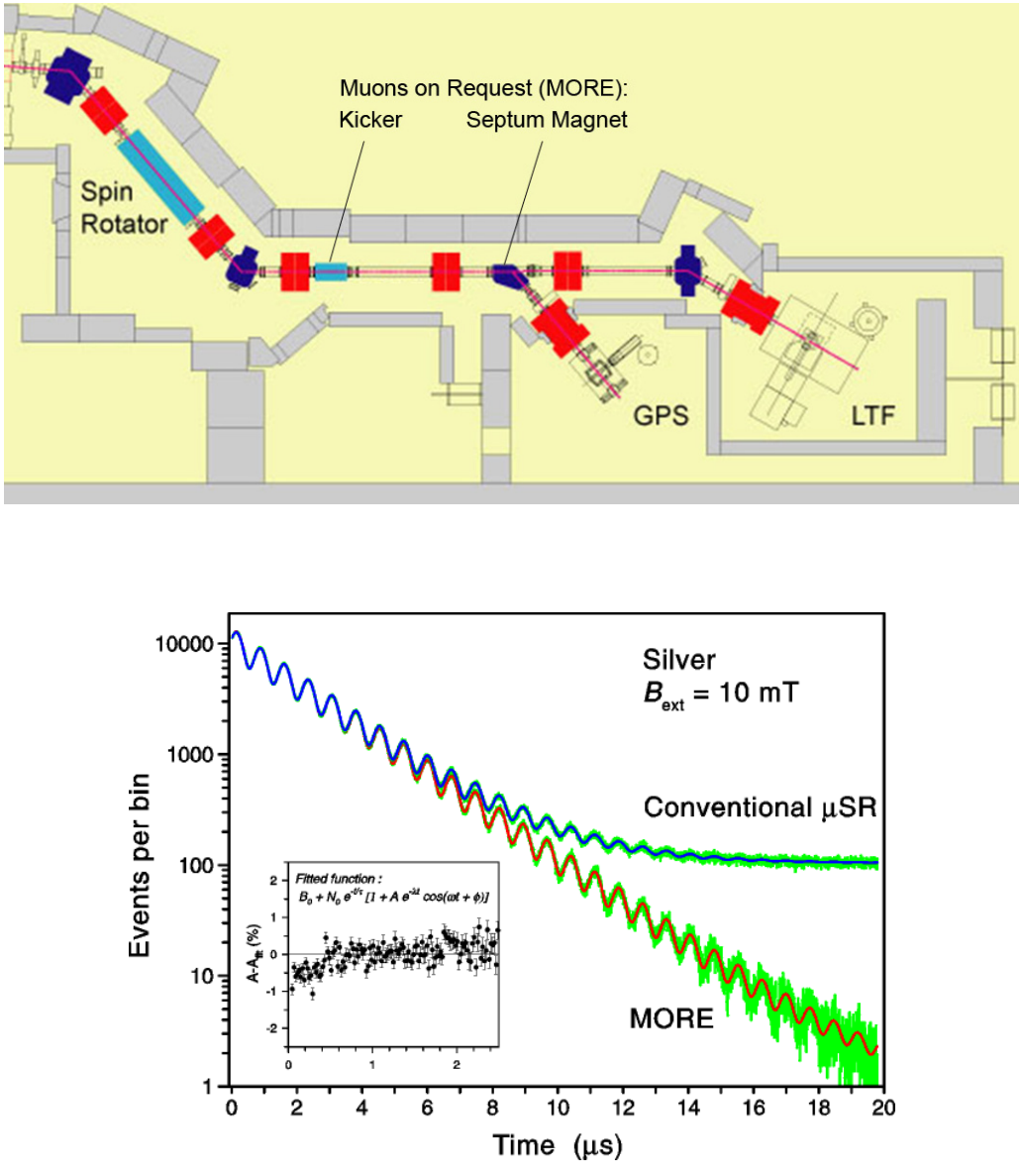

Fig. 5-6: Top: Layout of the GPS/LTF beam areas at PSI with Spin Rotator and MORE. Bottom: Example of µSR in silver in an external magnetic field of 10mT, taken with the GPS instrument (General Purpose Spectrometer) at PSI in MORE mode. For comparison a conventional spectrum taken at the same event rate is shown. The background in MORE mode is at least a factor of 100 lower than in conventional mode, thus easily allowing the study of muon-spin precession and relaxation up to 20µs. Insert: Reduced asymmetry plot for the first 2µs in MORE mode.

	Conventional	MORE	Pulsed μSR
Trigger	none	GPS	50 Hz
B_0/N_0 [10^{-5}]	660	8.7	ca. 1
Time resol. [ns]	<1	<1	80
Event. rate [10^6/h]	12	20	20-100

Table: Comparison of results obtained with GPS in conventional and in MORE mode (using the GPS muon-counter as trigger). Values for pulsed μSR (at ISIS Rutherford Appleton Laboratory, UK) are also shown.

After background subtraction the number of events in a detector placed in direction $\hat{n}$ (normally defined by the direction of the incoming muon beam or of the initial polarization):

$$N_{e^+}(t) = N_0 e^{-\frac{t}{\tau_\mu}} (1 + A_0 \vec{P}(t)\hat{n}) \qquad [5\text{-}3]$$

$$\vec{P}(t)\hat{n} = P(t) = \frac{< \vec{I}(t) \cdot \hat{n} >}{|\vec{I}(0)|}$$

e.g. for forward (F: forward with respect to muon spin $\vec{I}$) and backward (B) detectors we have:

$$N_F(t) = N_0 e^{-\frac{t}{\tau_\mu}} (1 + A_0 \vec{P}(t) \cdot \hat{n}_F)$$
$$N_B(t) = N_0 e^{-\frac{t}{\tau_\mu}} (1 + A_0 \vec{P}(t) \cdot \hat{n}_B) = N_0 e^{-\frac{t}{\tau_\mu}} (1 - A_0 \vec{P}(t) \cdot \hat{n}_F) \qquad [5\text{-}4]$$

The asymmetry A(t) is obtained from:

$$A(t) = A_0 P(t) = \frac{N_F(t) - N_B(t)}{N_F(t) + N_B(t)} \qquad [5\text{-}5]$$

A_0 is a parameter to be determined experimentally. It depends on factors such as detector solid angle, efficiency, absorption and scattering of positrons in the materials on the way from sample to detector. Generally $A_0 < 1/3$ (intrinsic decay asymmetry). Typical values lie between 0.25 and 0.3.
The function A(t) contains the information about the physics. In a real spectrometer one has to consider that the solid angles and efficiencies of the detectors may be different. This is taken care of by introducing in [5-5] one or two additional (fit) parameters (so called α, most important, and β parameters) (see exercise).

One distinguishes between transverse field- (TF) ($\vec{B}_{ext} \perp \vec{P}(0)$ longitudinal field- (LF, $\vec{B}_{ext} \parallel \vec{P}(0)$) or zero field measurements (ZF, $\vec{B}_{ext}=0$).

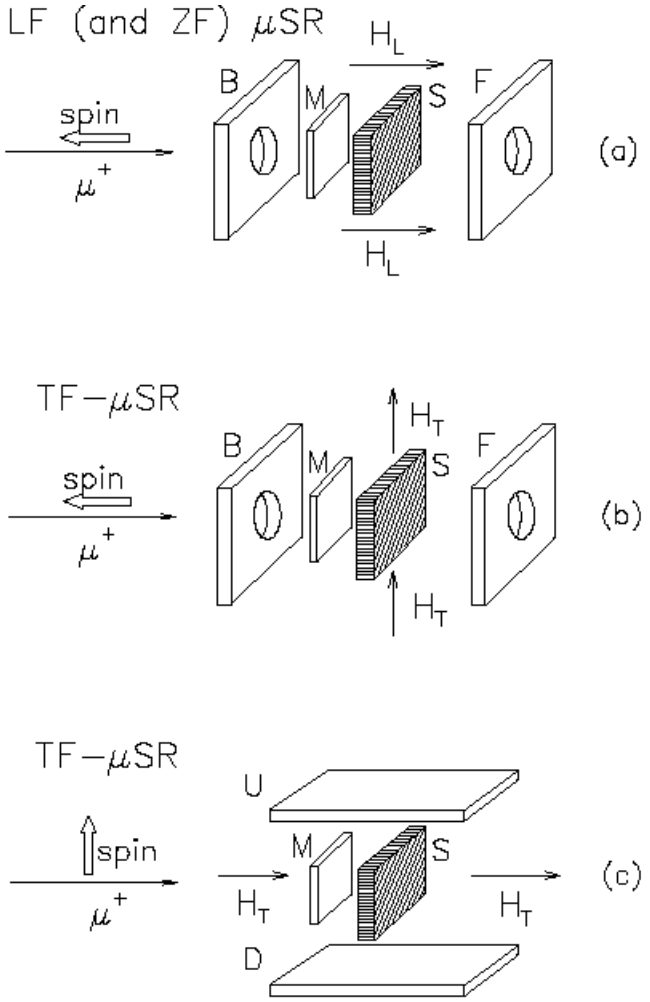

Fig. 5-7: a) Longitudinal (LF) and zero field geometry (ZF). b) and c) Transverse field geometry (TF)

Often the direction of $\vec{B}_{ext}$ is taken as z-axis. With $\vec{P}(0) \parallel \vec{n}$ then the measured polarization directions are indicated as:

In LF und ZF: $P_z(t)$
In TF $P_x(t)$

TF- spectrum and polarization function:

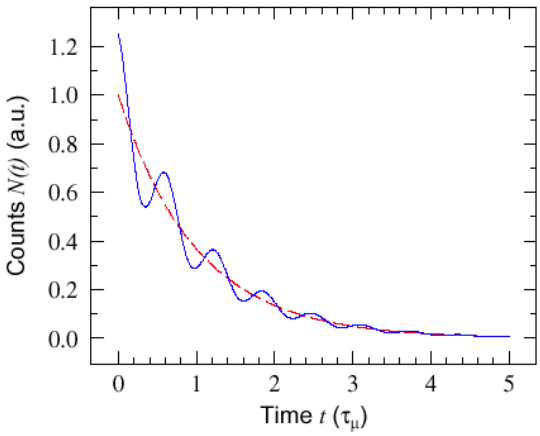

Positron count $N(t)$.

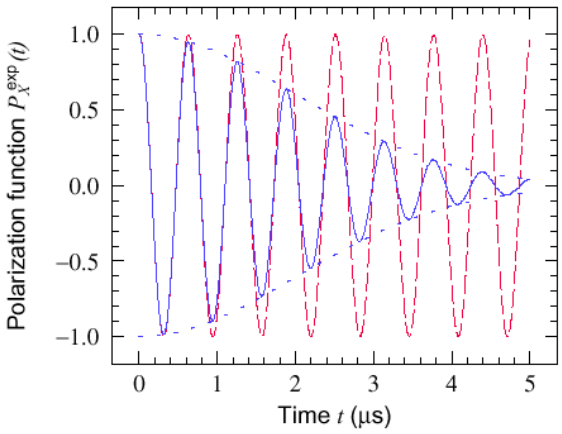

Two examples of transverse field polarisation function $P_X^{\exp}(t)$.

ZF and LF spectra and polarization function:

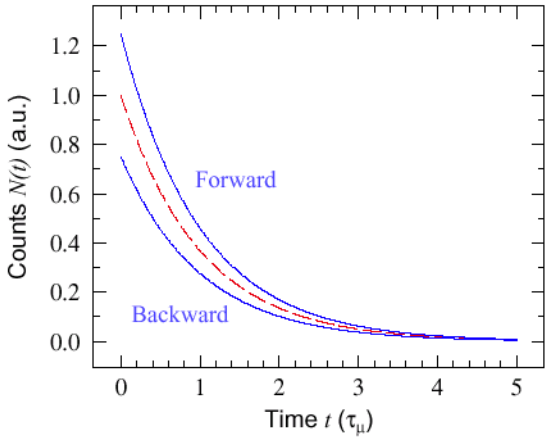

Positron counts $N_{\mathrm{F}}(t)$ and $N_{\mathrm{B}}(t)$.

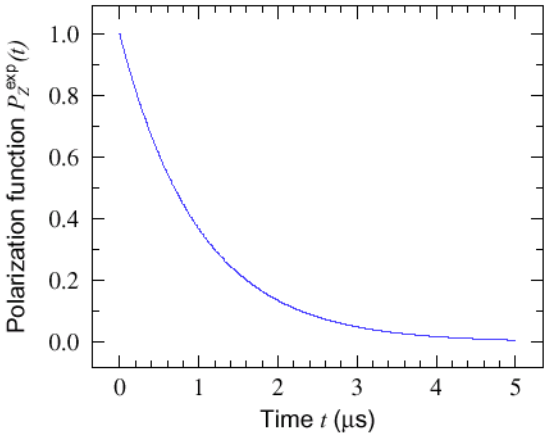

An example of a longitudinal field polarisation function $P_Z^{\exp}(t)$.

Fig. 5-8: Examples of μSR spectra and polarization functions.

5.1 Polarization- and relaxation functions for static fields

Spin precession in a static field.
Static means: the local field experienced by the muon is constant over times $t \gtrsim 5\text{-}20\ \tau_\mu$.

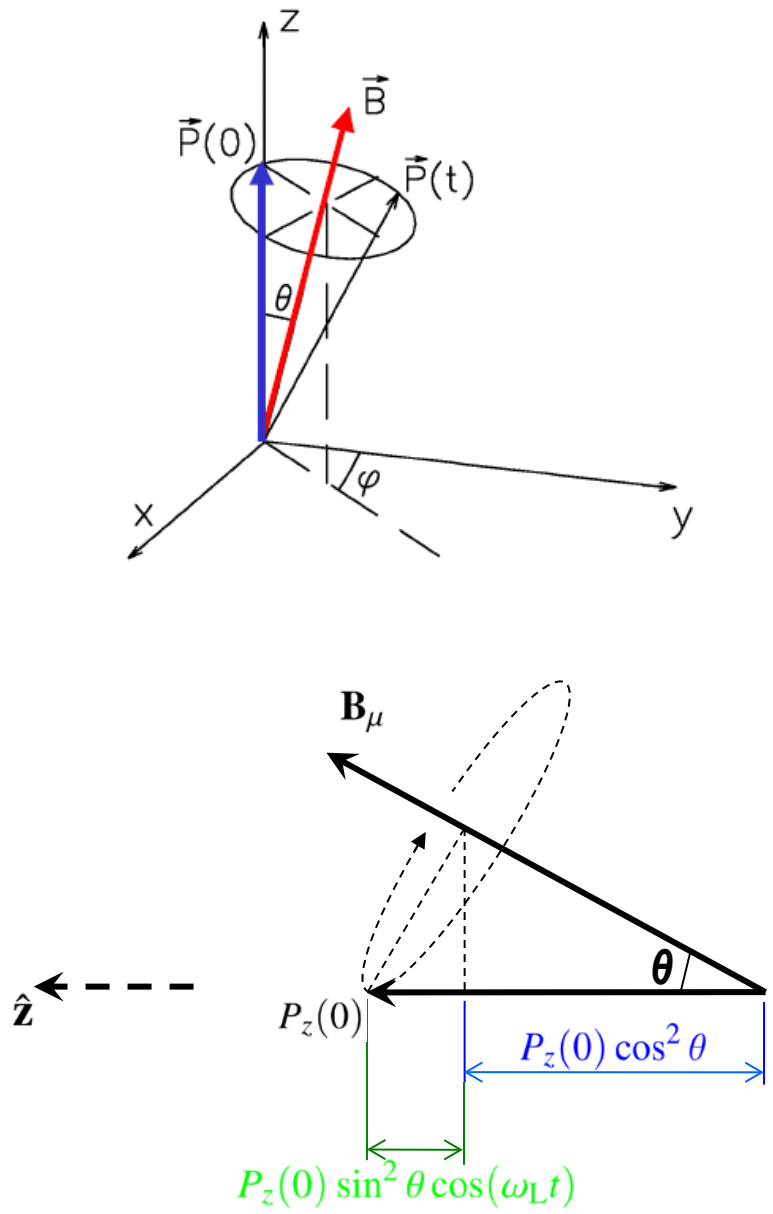

Fig. 5-9: Muon spin precession in a constant field ($\vec{B}$ or $\vec{B}_\mu$). The initial polarization is along the z-axis, which is also the observation direction ($\hat{n}$).

$$P(t) = \frac{< \vec{I}(t) \cdot \vec{I}(0) >}{\left|\vec{I}(0)\right|^2} \qquad [5\text{-}6]$$

$$P(t) = P_z(t) \equiv P_{\vec{B}}(t) = \cos^2\theta + \sin^2\theta\cos(\omega_L t) = \frac{B_z^{\,2}}{B^2} + \frac{B_x^{\,2} + B_y^{\,2}}{B^2}\cos(\gamma_\mu Bt)$$

$$P_y(t) = \frac{1}{2}\sin 2\theta \sin\varphi(1-\cos(\omega_L t)) - \sin\theta\cos\varphi\sin(\omega_L t) \qquad [5\text{-}7]$$

$$P_x(t) = \frac{1}{2}\sin 2\theta \cos\varphi(1-\cos(\omega_L t)) + \sin\theta\sin\varphi\sin(\omega_L t)$$

$$B = \sqrt{B_x^{\,2} + B_y^{\,2} + B_z^{\,2}}$$

By making use of Eq. [5-7], with a single crystal sample one can determine the direction of the internal fields from the angular dependence of the amplitudes of the oscillating components.
Example is a measurement of the tetragonal heavy fermion compound $CeRhIn_5$ (A. Schenck et al., Phys. Rev. B 66 (2002) 144404).

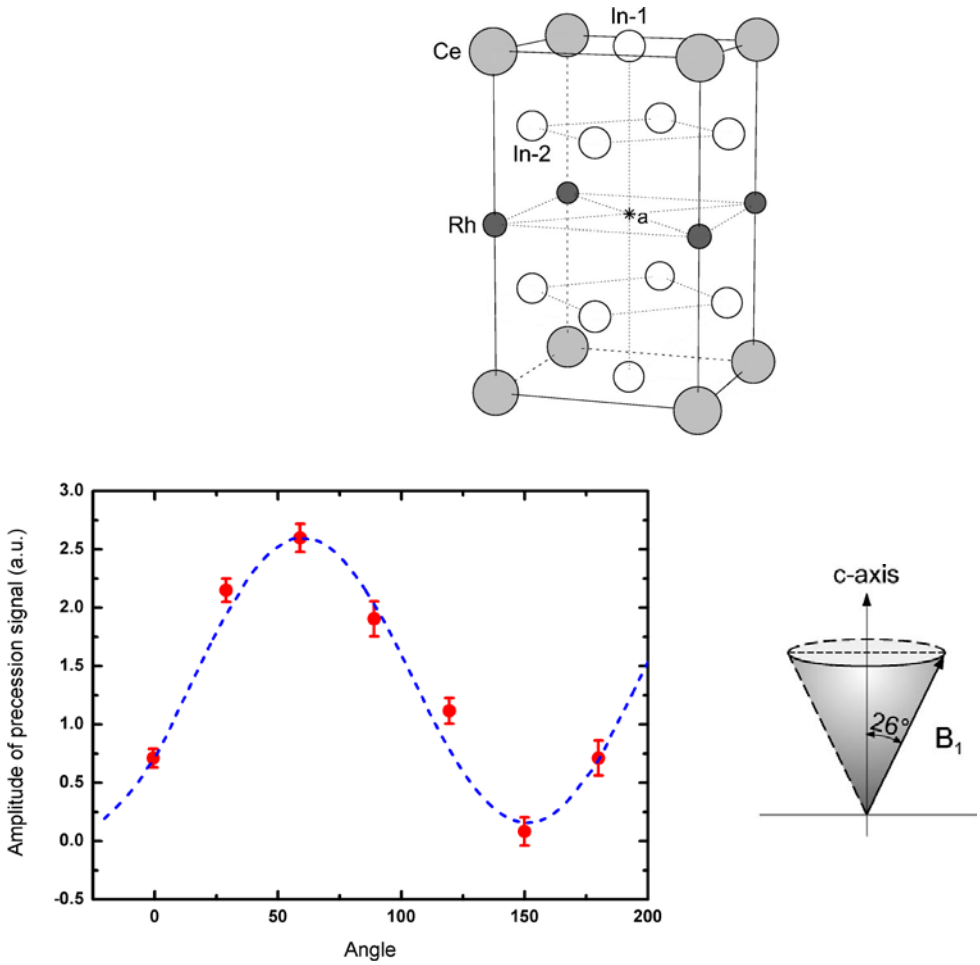

Fig. 5-10: Crystal structure of $CeRhIn_5$. Amplitude of the precession signal as a function of the rotation angle of the crystal. From the measurement a local field pointing at 26° with respect to the c-axis is determined. The local field in this case is produced by an incommensurate helical structure of the Ce moments and also induced moments at the Rh sites.

If the field distribution probed by the muon ensemble $p(\vec{B})$ is known we can calculate the corresponding polarization function:

$$P_z(t) = \frac{\int P_{\vec{B}}(t) p(\vec{B}) d^3B}{\int p(\vec{B}) d^3B}$$

This expression can be used to calculate the muon spin polarization in several special very useful cases.

A) Zero Field case with $\left|\vec{B}\right|$ *constant, random direction isotropically distributed* (e.g. in domain structures of ferromagnetic materials or in ferromagnetic or antiferromagnetic powder samples).

In this case:

$$p(\vec{B}) d^3B = \frac{1}{4\pi} \delta(B - B_\mu) dB d\Omega$$

$$P(t) = \frac{1}{4\pi} \int \left(\cos^2\theta + \sin^2\theta \cos(\omega_L t) \right) d(\cos\theta) d\phi = \frac{1}{3} + \frac{2}{3} \cos(\gamma_\mu B_\mu t) \qquad [5\text{-}8]$$

If the fields are isotropic in the xz or yz planes, we obtain $P_z(t) = \frac{1}{2} + \frac{1}{2} \cos(\gamma_\mu B_\mu t)$

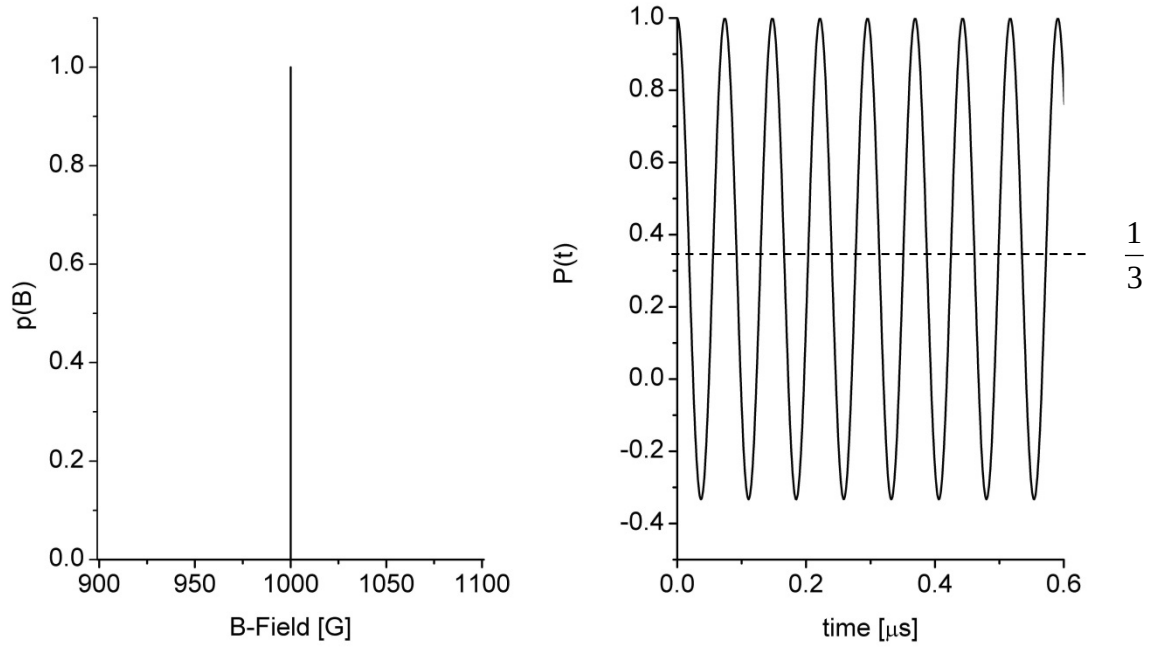

Fig 5-11: Polarization and corresponding magnetic field distribution in the case of equation [5-8].

Eq. [5-8] and Fig. 5-11 correspond to the ideal case. In the real case, there is distribution of fields around a mean value; i.e. the field distribution is not a delta function but has a finite width, better described e.g. by a Gaussian or Lorentz distribution. In the case of a Gaussian field distribution of width $< \Delta B_x^2 >=< \Delta B_y^2 >=< \Delta B_z^2 >\equiv< \Delta B^2 >$ small compared to the average field B_μ, [5-8] becomes for instance:

$$P(t) = \frac{1}{3} + \frac{2}{3} e^{-\frac{1}{2}\gamma_\mu^2 \langle \Delta B^2 \rangle t^2} \cos(\gamma_\mu B_\mu t)$$

$< \Delta B^2 >=< (B_i - < B_i >)^2 >$, i=x,y,z $< \Delta B_x^2 >=< \Delta B_y^2 >=< \Delta B_z^2 >$

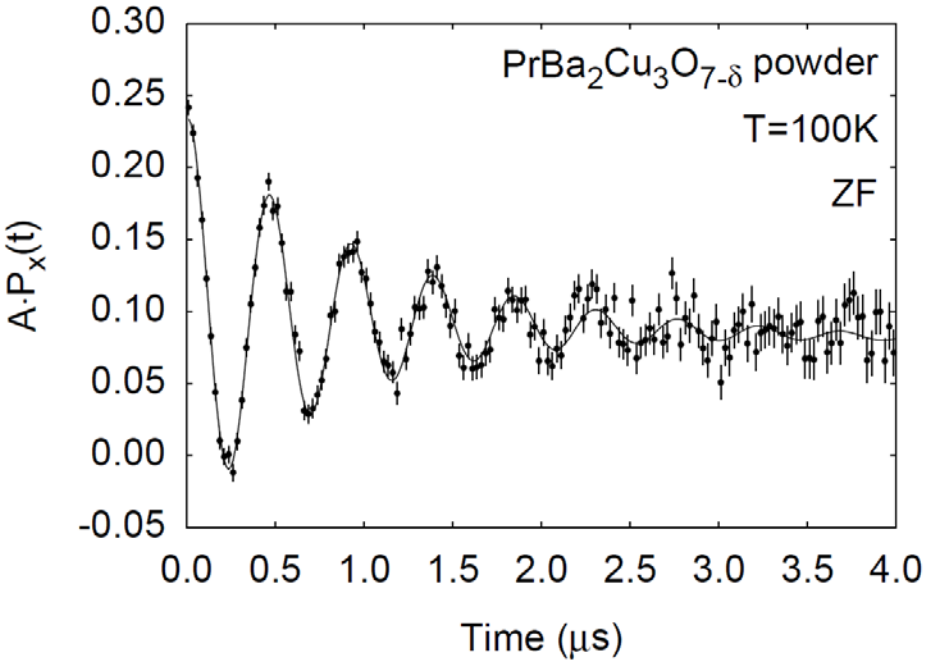

Fig 5-12: Polycrystalline $PrBa_2Cu_3O_{7-\delta}$, ZF measurement, AF order of the Cu moments. The asymmetry shows the 2/3 precessing component (damped) and the 1/3 non-precessing component (B.M. Wojek et al, Physica B **404**, 720 (2009)).

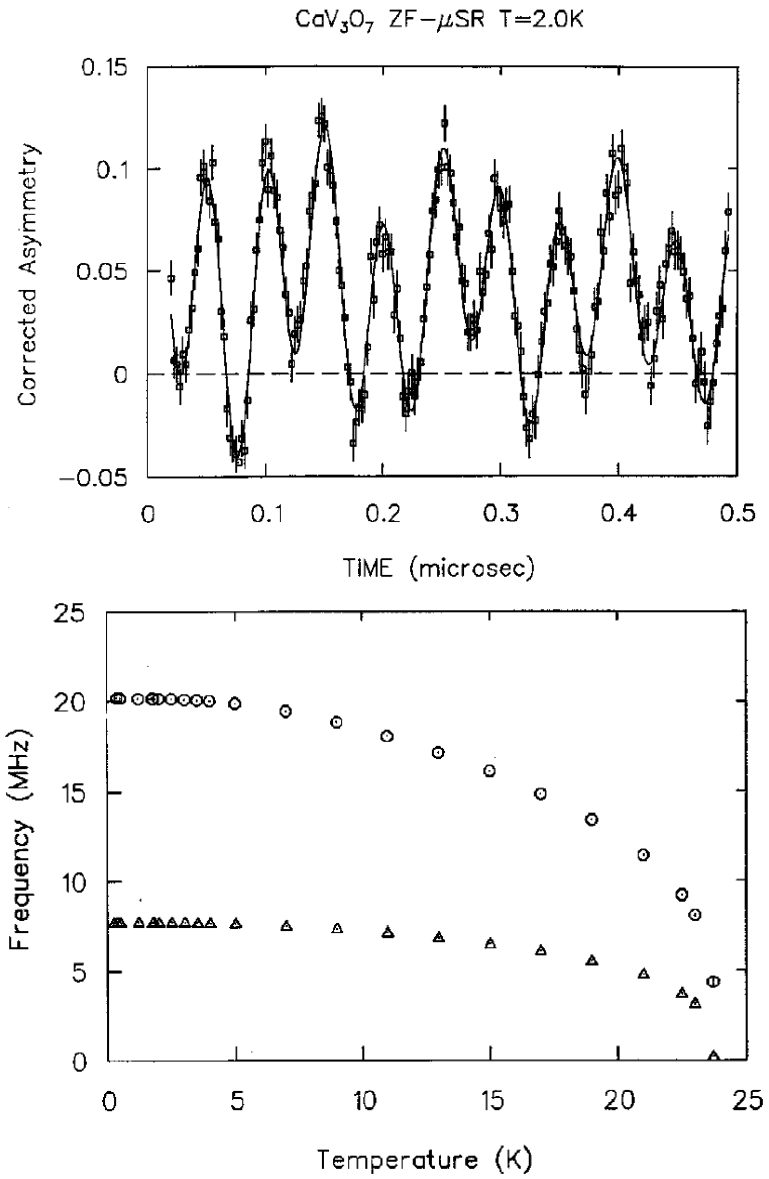

Fig 5-13: ZF μSR spectra in the CaV_3O_7 antiferromagnet. The local field is a consequence of the AF order of the V moments. We observe two precession signals corresponding to two different muon sites and in addition the non-precessing 1/3 component. The bottom curve shows the corresponding microscopic magnetization curve (R.E. Walstedt, L.R. Walker, Phys. Rev. **9** 4857 (1974)).

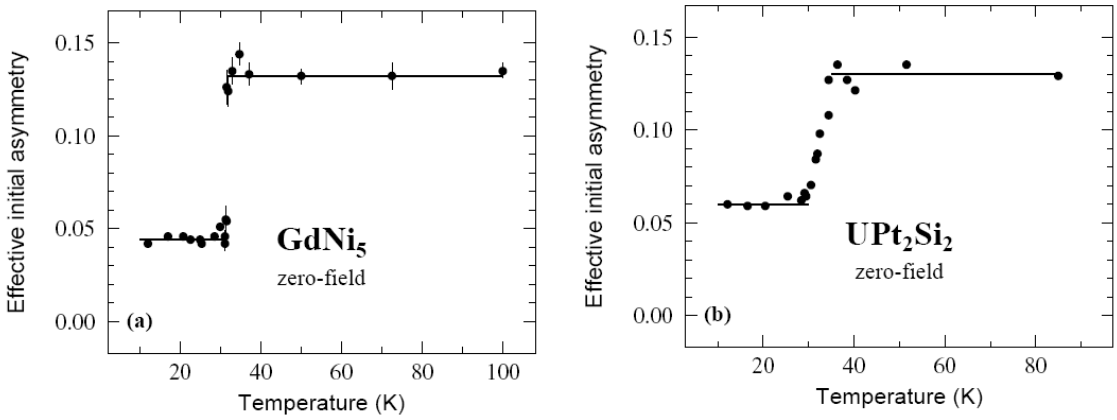

Fig 5-14: Zero field measurement. Initial asymmetry A(0) as a function of temperature in two polycrystalline samples. a) $GdNi_5$ (ferromagnet) b) UPt_2Si_2 (antiferromagnet). At T_c and T_N respectively the asymmetry falls to 1/3 (from P. Dalmas de Réotier, A. Yaouanc, Journal of Physics, Cond. Matt. **9**, R9113 (1997)). The origin of the jump can be the formation of large local fields or of fluctuating moments, so that the precessing 2/3 part of the polarization is suppressed.

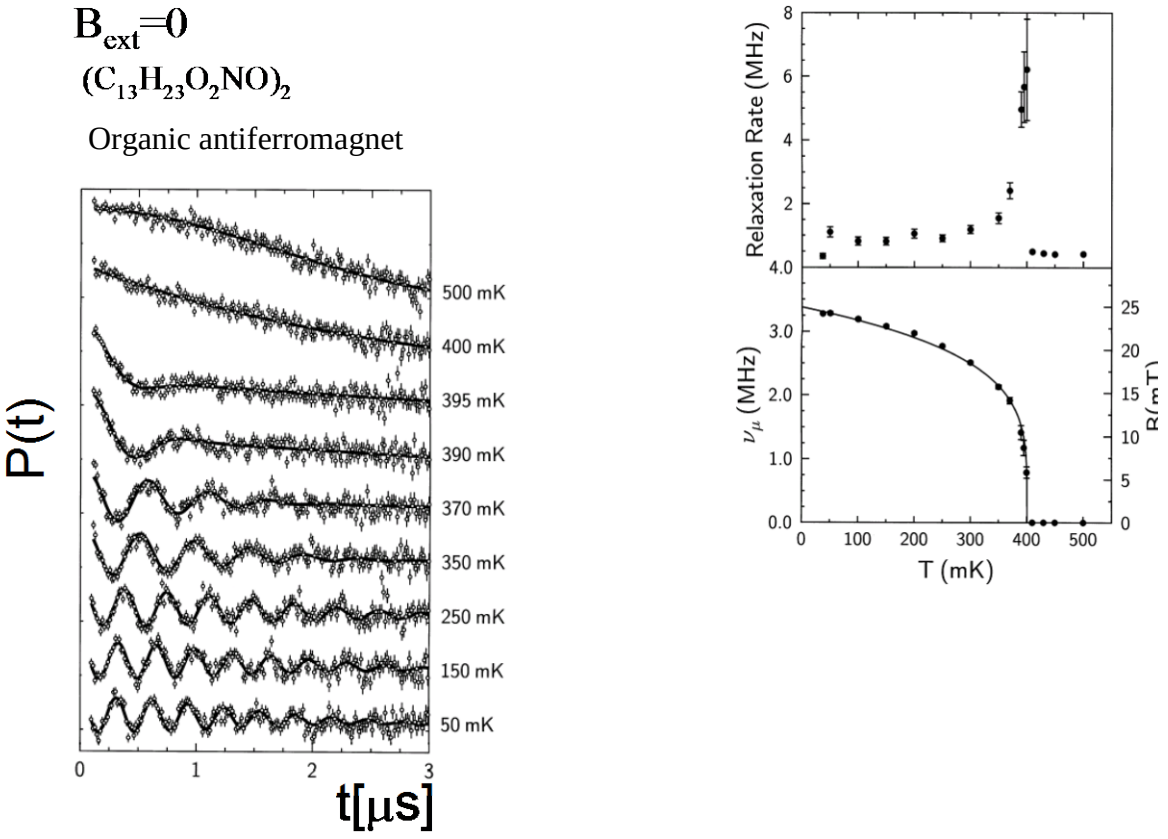

Fig 5-15: ZF μSR spectra in an organic antiferromagnet, showing the magnetic phase transition (S. Blundell et al., Physica B 289, 115 (2000)). The T-dependence of the spontaneous precession frequency gives the local magnetization. The peak in the relaxation rate λ(T) at T_N is typical of a phase transition. In this case only the local magnetization is of interest so that $P(t) \approx A_L + A_T e^{-\lambda(T)t} \cos(2\pi\nu_\mu(T)t + \varphi)$.

B) $\vec{B}$ *Gauss distributed in x, y and z direction* with

$< B_i >=0$ and $\qquad i = x,y,z$

$$< \Delta B_i^2 >=< (B_i - < B_i >)^2 > \; = \; < B_i{}^2 > - < B_i >^2 = \; < B_i{}^2 > \; = \frac{\sigma^2}{\gamma_\mu^2} \qquad [5\text{-}9]$$

A Gauss distribution of fields is obtained in the case of a dense arrangement of randomly oriented moments (for example nuclear moments, which on the μSR time scale can be considered as static) and is justified by the central limit theorem.

Magnetic field distribution:

$$p^G(B_i) = \frac{\gamma_\mu}{\sqrt{2\pi}\sigma} e^{-\frac{\gamma_\mu^2 B_i^2}{2\sigma^2}} \qquad i = x,y,z \qquad [5\text{-}10]$$

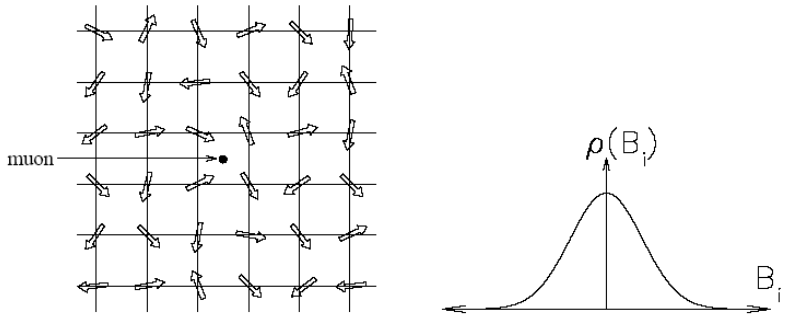

Fig. 5-16 a) Randomly oriented dense moments. b) Resulting distribution of fields projected onto an axis. The projection is a Gaussian distribution in each of the field components.

The distribution function for the absolute value $\left|\vec{B}\right| \equiv B$ is

$$p^G(B)dB = (\frac{\gamma_\mu}{\sqrt{2\pi}\sigma})^3 e^{-\frac{\gamma_\mu^2 B^2}{2\sigma^2}} \cdot 4\pi B^2 dB \qquad [5\text{-}11]$$

Which is a Maxwell distribution with maximum at $B = \sqrt{2}\frac{\sigma}{\gamma_\mu}$ and $< B > \approx \sqrt{\frac{8}{\pi}}\frac{\sigma}{\gamma_\mu}$.

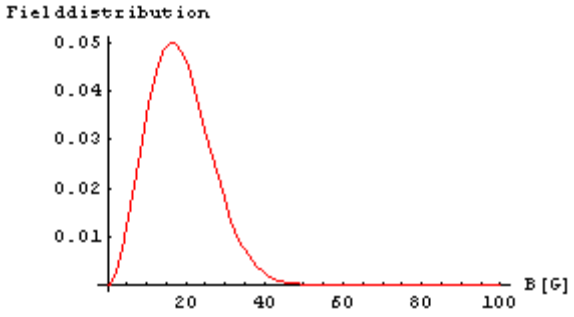

Fig. 5-17: Distribution of the field value p(B) for Gauss distributed B_x, B_y and B_z (σ=1 μs^{-1}).

The relaxation function is obtained in this case from:

$$P^{G-KT}(t) = \int p^G(B_x)p^G(B_y)p^G(B_z)P_{\vec{B}}(t)dB_x dB_y dB_z \qquad [5\text{-}12]$$

Where $P_{\vec{B}}(t)$ is given by [5-7].

The integration in [5-12] can be explicitly performed, by using for instance spherical coordinates. We obtain the well-known Kubo-Toyabe relaxation function (Fig. 5-19) (R. Kubo and T. Toyabe in *Magnetic Resonance and Relaxation*, edited by R. Blinc . North-Holland, Amsterdam, 1967):

$$P^{G\text{-}KT}(t) = \frac{1}{3} + \frac{2}{3}(1-\sigma^2t^2)e^{-\frac{\sigma^2t^2}{2}} \qquad [5\text{-}13]$$

Damped oscillation (with damping σ, relaxation rate) around maximum of $|\vec{B}|$

On average one third of the muons does not precess or relax.

The 1/3 and 2/3 components can be qualitatively understood by considering that the local field is random in all directions: about 1/3 is parallel or antiparallel to the muon spin and about 2/3 is perpendicular.
In the paramagnetic state, a Kubo-Toyabe function is very often observed reflecting the field distribution of the small fields created by the nuclear moments.

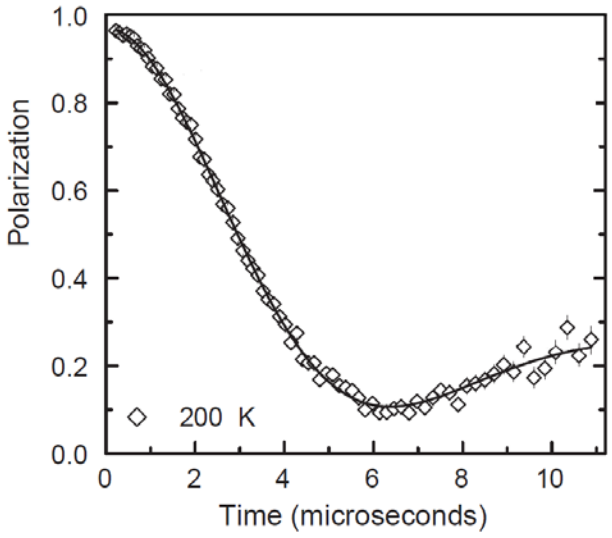

Fig. 5-18: Observation of a Gauss Kubo-Toyabe relaxation in semiconducting InN, Y.G. Celebi et al., Physica B 340-342, 385 (2003).

C) If the *local fields instead of Gauss are Lorentz distributed*:

$$p^{L}(B)dB = \left(\frac{\gamma_{\mu}^{3}}{\pi^{2}}\right) \frac{a}{(a^{2}+\gamma_{\mu}^{2}B^{2})^{2}} \cdot 4\pi B^{2} dB$$

One obtains the so called *static Lorentz Kubo-Toyabe function (ZF)*:

$$P^{L-KT}(t) = \frac{1}{3} + \frac{2}{3}(1-at)e^{-at} \qquad [5\text{-}14]$$

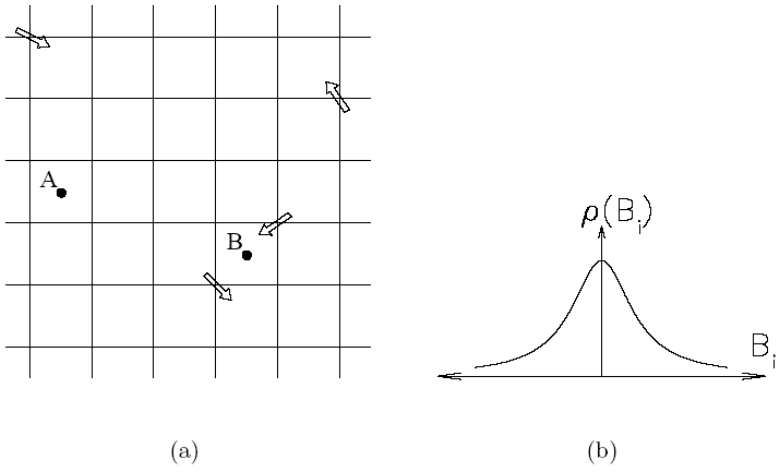

Fig. 5-19: a) Randomly oriented dilute moments. Muons at site A feel weak fields, while those at B feel stronger fields. b) Resulting distribution of fields projected onto an axis. The projection is a Lorentzian distribution.

It holds:

$$p^L(B_x) = \int\int p^L(B)dB_y dB_z = (\frac{\gamma_\mu}{\pi})\frac{a}{(a^2+\gamma_\mu^2 B_x^2)}$$

($\frac{a}{\gamma_\mu}$ = HWHM)

and in analogy for B_y and B_z.

But differently from the Gaussian case:

$$p^L(B)dBd\Omega \neq p^L(B_x)p^L(B_y)p^L(B_z)dB_x dB_y dB_z$$

Sometimes a general relaxation function, which in the limiting case gives the Gauss and Lorentz Kubo-Toyabe function, is used:

$$P^{Gen-KT}(t) = \frac{1}{3} + \frac{2}{3}(1-\lambda^\alpha t^\alpha)e^{-\frac{\lambda^\alpha t^\alpha}{\alpha}} \qquad 1 \leq \alpha \leq 2$$

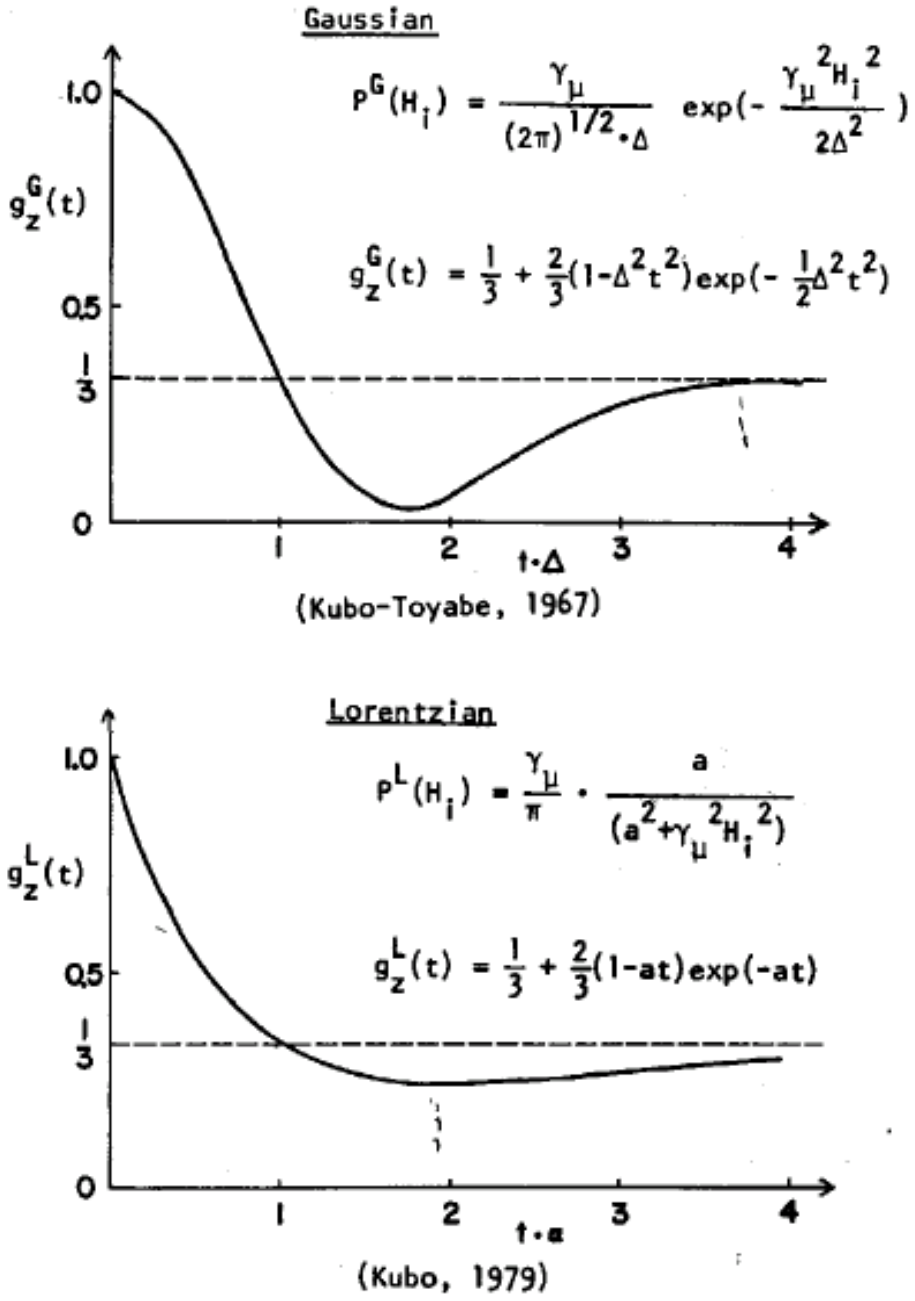

Fig. 5-20: Static ZF polarization functions, corresponding to Gaussian and Lorentzian field distributions.

D) Longitudinal field case

LF Gauss KT: as example B) but in addition an external field $\vec{B}_{ext} \| \hat{z}$ is applied. In this case the (total) field distribution modifies to:

$$p^{G}(B_z) = \frac{\gamma_\mu}{\sqrt{2\pi\sigma}} e^{-\frac{\gamma_\mu^2 (B_{ext} - B_z)^2}{2\sigma^2}} \qquad [5\text{-}15]$$

The B_x and B_y distributions remain unchanged and the B_z distribution is offset. If we integrate [5-12] with the new distribution we get the so called Gauss-Kubo-Toyabe relaxation in longitudinal field (R.S. Hayano et al., Phys. Rev. **B20**, 850 (1979)).

$$P^{G-KT}(t, B_{ext}) = 1 - \frac{2\sigma^2}{(\gamma_\mu B_{ext})^2}\left[1 - e^{-\frac{\sigma^2 t^2}{2}} \cos(\gamma_\mu B_{ext} t)\right] + \frac{2\sigma^4}{(\gamma_\mu B_{ext})^3} \int_0^t e^{-\frac{\sigma^2 t^2}{2}} \sin(\gamma_\mu B_{ext} t')dt' \qquad [5\text{-}16]$$

If B_{ext} is large with respect to the local fields the spin will be aligned along the z-direction (so called *decoupling* of static fields). LF measurements are used to distinguish between static and dynamic contributions to the relaxation.

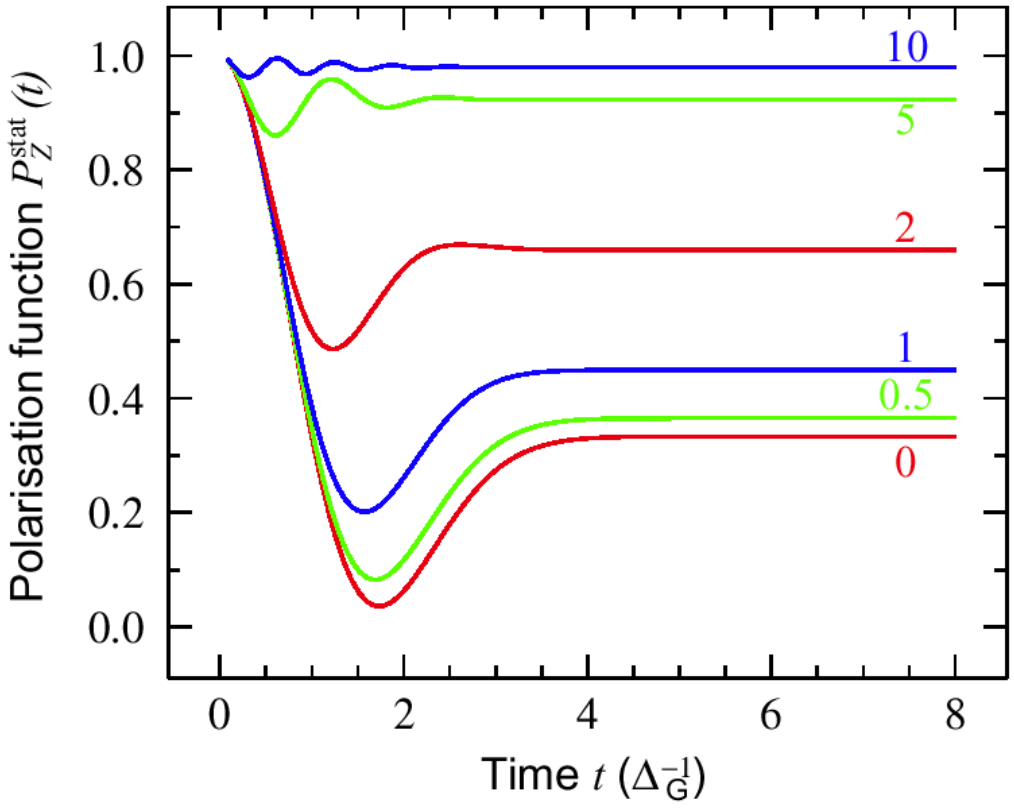

Fig. 5-21: Field dependence of the polarization function for isotropic Gauss distributed fields. Time scale in units of $1/\sigma$. B_{ext} in units of σ/γ_μ. The zero field curve corresponds to the Kubo-Toyabe function.

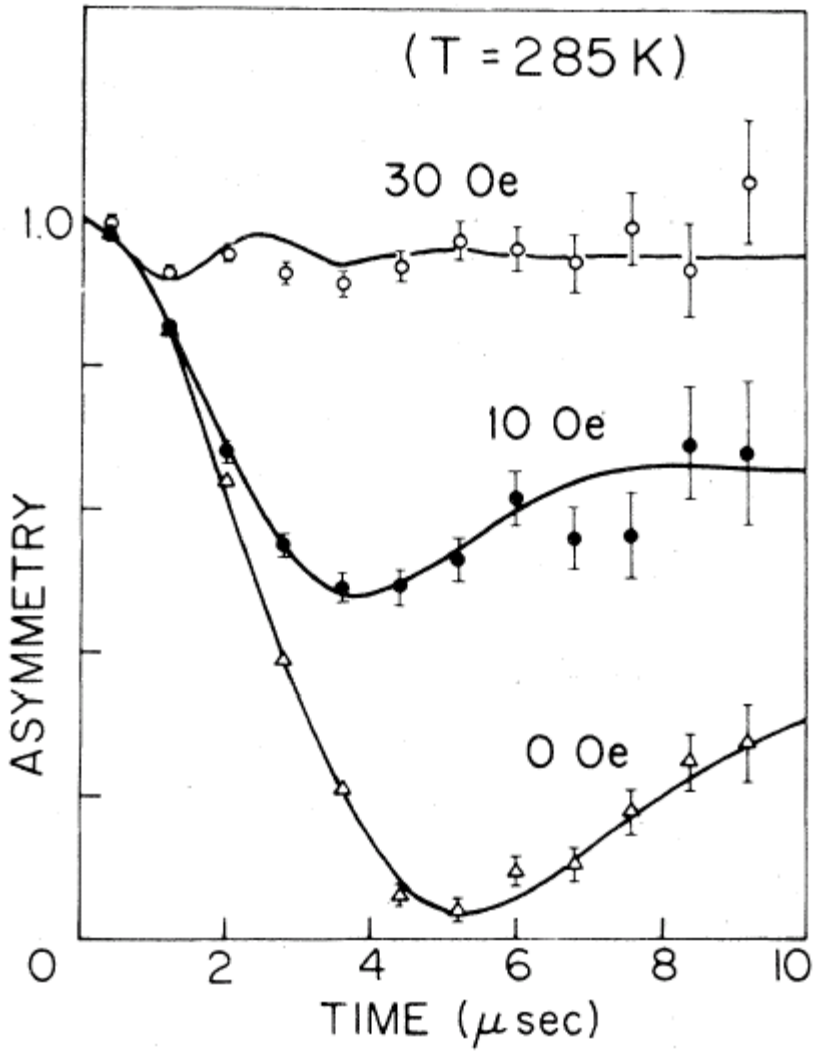

$$t_{min} = \frac{\sqrt{3}}{\sigma} \quad \left(P(t_{min}) = 0.03583\right)$$

Fig 5-22: Example of Gauss Kubo-Toyabe relaxation and longitudinal field-decoupling: Muon spin relaxation in the paramagnetic phase of MnSi (R.S. Hayano et al., Phys. Rev B **20**, 850 (1979)). The local field is produced in this case mainly by the Mn nuclear moments.

The behavior of the LF relaxation can be understood qualitatively by considering that the 1/3 component of eq. [5-8] corresponding to the muons with spin parallel or antiparallel to the local field is increased in B_{ext}, whereas the 2/3 component is reduced while still showing indication of a precession around the external field.

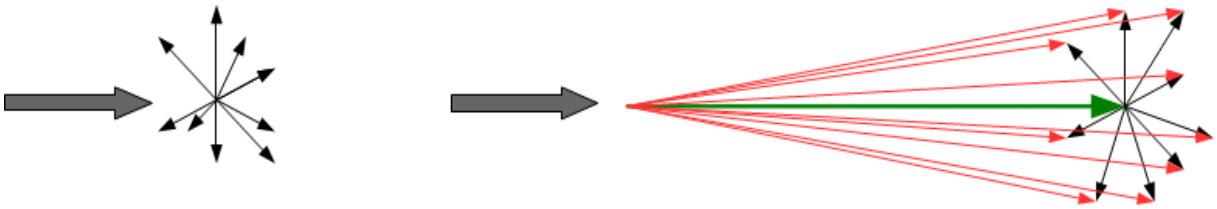

$B_{ext} = 0$ $B_{ext} \neq 0$

E) *LF with Lorentz distributed local fields,* $\vec{B}_{ext} \| \hat{z}$.

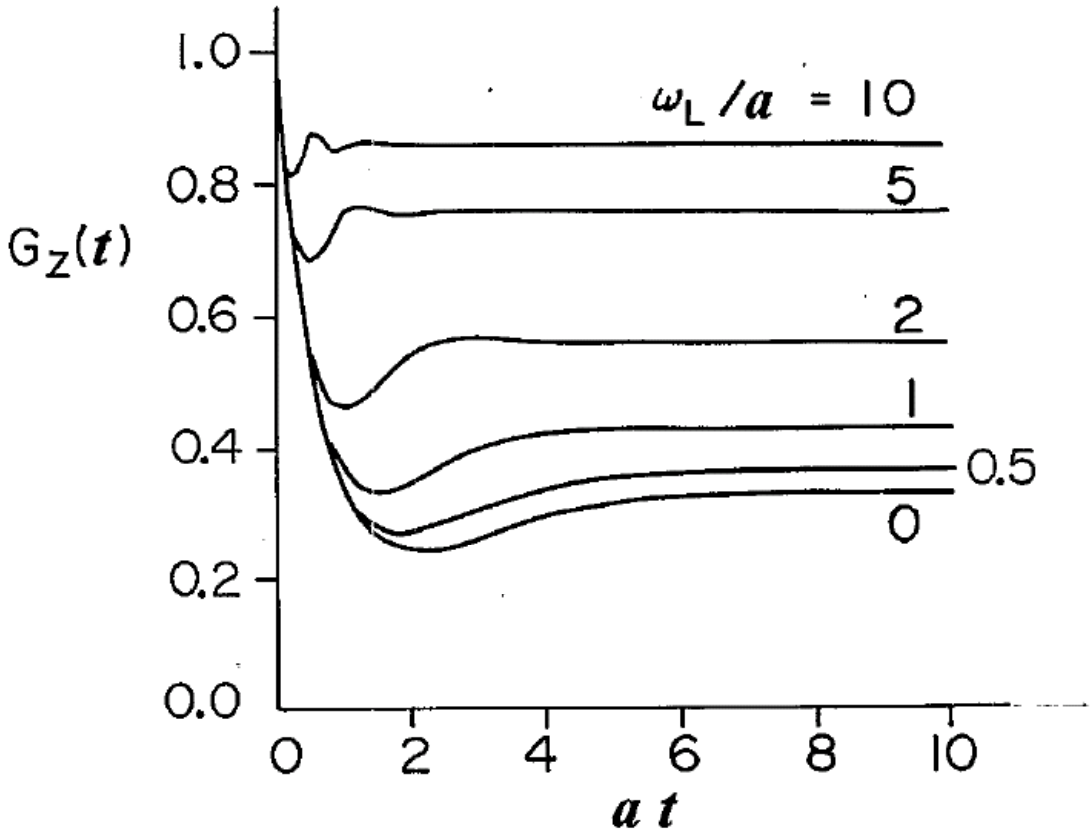

Fig. 5-23: $G_z(t)$: Muon spin polarization in random distributed Lorentz fields as function of the external field (ω_L / γ_μ) (Y. Uemura et al., Phys. Rev. **B31**, 546 (1985)).

$$P^{L-KT}(t, B_{ext}) = 1 - \frac{a}{(\gamma_\mu B_{ext})} j_1(\gamma_\mu B_{ext} t) e^{-at} - \left(\frac{a}{\gamma_\mu B_{ext}}\right)^2 \left[j_0(\gamma_\mu B_{ext} t) e^{-at} - 1 \right] - \left[1 + \left(\frac{a}{\gamma_\mu B_{ext}}\right)^2 \right] a \int_0^t j_0(\gamma_\mu B_{ext} t') e^{-at'} dt' \qquad [5\text{-}17]$$

j_0 and j_1 are spherical Bessel functions.

F) Transverse field case. $\vec{B}_{ext} \perp \vec{P}(0)$ and $\parallel \hat{z}$. *Relaxation in an external field:*

If the internal fields are Gauss distributed, we have

$$p^G(\vec{B}) = \frac{\gamma_\mu}{\sqrt{2\pi}\sigma} e^{-\frac{\gamma_\mu^2 B_x^{\,2}}{2\sigma^2}} \frac{\gamma_\mu}{\sqrt{2\pi}\sigma} e^{-\frac{\gamma_\mu^2 B_y^2}{2\sigma^2}} \frac{\gamma_\mu}{\sqrt{2\pi}\sigma} e^{-\frac{\gamma_\mu^2 (B_{ext}-B_z)^2}{2\sigma^2}} \qquad [5\text{-}18]$$

with $\left|\vec{B}_{ext}\right| >> \frac{\sigma}{\gamma_\mu}$, in [5-7]: $\theta = 90$, $P_{\vec{B}}(t) = \cos(\gamma_\mu B t)$ and $\gamma_\mu B \simeq \gamma_\mu B_z$

$$P^{G-TF}(t) = \int p^G(B_z) p^G(B_y) p^G(B_x) P_{\vec{B}}(t) dB_x dB_y dB_z$$

$$\cong \left[\int \left(\frac{\gamma_\mu}{\sqrt{2\pi}\sigma}\right)^3 e^{-\frac{\gamma_\mu^2 (B_{ext}-B_z)^2}{2\sigma^2}} \cos(\gamma_\mu B_z t) dB_z \int e^{-\frac{\gamma_\mu^2 B_y^2}{2\sigma^2}} e^{-\frac{\gamma_\mu^2 B_x^2}{2\sigma^2}} dB_y dB_x \right] = \qquad [5\text{-}19]$$

$$= e^{-\frac{\sigma^2 t^2}{2}} \cos(\gamma_\mu B_{ext} t)$$

The Gauss relaxation does not depend on B_{ext} if $\left|\vec{B}_{ext}\right| >> \frac{\sigma}{\gamma_\mu}$. Fig. 5.8a shows an example of Gauss relaxation (depolarization due to dephasing, inhomogeneous broadening).

G) If the local field is *Lorentz-* instead of *Gauss distributed*, we obtain:

$$P^{L-TF}(t) = e^{-at} \cos(\gamma_\mu B_{ext} t) \qquad [5\text{-}20]$$

In both cases the oscillation frequency gives the average local field (in this case B_{ext}) and the damping gives the local field width.

Depending on the physical conditions, there may be various contributions to the average field, which is then not given simply by the external field. An example is the Knight shift K where $B_{ext} \rightarrow B_{ext}(1+K)$, another example is the vortex state in a superconductor, where $B_{ext} \rightarrow \langle B \rangle$, average field generated by the vortices, see Chapt. 7.

In the static TF case, when $\langle B_z \rangle >> \frac{\sigma}{\gamma_\mu} = \sqrt{\langle \Delta B_z^2 \rangle}$, a Gauss relaxation reflects a Gauss distribution of local fields and an exponential relaxation reflects a Lorentz distribution of local fields (polarization and field distribution are related via a cosine Fourier transform).